



HAL
open science

Dynamic Heterogeneities in Liquid Mixtures Confined in Nanopores

Ramona Mhanna, Pierre Catrou, Sujeet Dutta, Ronan Lefort, Ilham Essafri, Aziz Ghoufi, Matthias Muthmann, Michaela Zamponi, Bernhard Frick, Denis Morineau

► **To cite this version:**

Ramona Mhanna, Pierre Catrou, Sujeet Dutta, Ronan Lefort, Ilham Essafri, et al.. Dynamic Heterogeneities in Liquid Mixtures Confined in Nanopores. *Journal of Physical Chemistry B*, 2020, 124 (15), pp.3152-3162. 10.1021/acs.jpcc.0c01035 . hal-02523643

HAL Id: hal-02523643

<https://hal.science/hal-02523643>

Submitted on 29 Mar 2020

HAL is a multi-disciplinary open access archive for the deposit and dissemination of scientific research documents, whether they are published or not. The documents may come from teaching and research institutions in France or abroad, or from public or private research centers.

L'archive ouverte pluridisciplinaire **HAL**, est destinée au dépôt et à la diffusion de documents scientifiques de niveau recherche, publiés ou non, émanant des établissements d'enseignement et de recherche français ou étrangers, des laboratoires publics ou privés.

Dynamic Heterogeneities in Liquid Mixtures Confined in Nanopores

Ramona Mhanna, Pierre Catrou, Sujeet Dutta, Ronan Lefort, Ilham Essafri, Aziz Ghoufi, Matthias Muthmann, Michaela Zamponi, Bernhard Frick, and Denis Morineau

J. Phys. Chem. B, **Just Accepted Manuscript** • DOI: 10.1021/acs.jpcc.0c01035 • Publication Date (Web): 27 Mar 2020

Downloaded from pubs.acs.org on March 29, 2020

Just Accepted

“Just Accepted” manuscripts have been peer-reviewed and accepted for publication. They are posted online prior to technical editing, formatting for publication and author proofing. The American Chemical Society provides “Just Accepted” as a service to the research community to expedite the dissemination of scientific material as soon as possible after acceptance. “Just Accepted” manuscripts appear in full in PDF format accompanied by an HTML abstract. “Just Accepted” manuscripts have been fully peer reviewed, but should not be considered the official version of record. They are citable by the Digital Object Identifier (DOI®). “Just Accepted” is an optional service offered to authors. Therefore, the “Just Accepted” Web site may not include all articles that will be published in the journal. After a manuscript is technically edited and formatted, it will be removed from the “Just Accepted” Web site and published as an ASAP article. Note that technical editing may introduce minor changes to the manuscript text and/or graphics which could affect content, and all legal disclaimers and ethical guidelines that apply to the journal pertain. ACS cannot be held responsible for errors or consequences arising from the use of information contained in these “Just Accepted” manuscripts.

Dynamic Heterogeneities in Liquid Mixtures Confined in Nanopores

Ramona Mhanna,^{†,§} Pierre Catrou,[†] Sujeet Dutta,[†] Ronan Lefort,[†] Ilham Essafri,[†] Aziz Ghoufi,[†]

Matthias Muthmann,[‡] Michaela Zamponi,[‡] Bernhard Frick,[§] Denis Morineau^{†*}

[†]Institute of Physics of Rennes, CNRS-University of Rennes 1, UMR 6251, F-35042 Rennes,
France

[§] Institut Laue-Langevin, 71 avenue des Martyrs, F-38000 Grenoble, France

[‡] Forschungszentrum Jülich GmbH, Jülich Centre for Neutron Science at MLZ

Lichtenbergstr. 1, 85748 Garching, Germany

Corresponding Author

* E-mail: denis.morineau@univ-rennes1.fr

ABSTRACT: Binary liquid mixtures can exhibit nanosegregation, albeit being fully miscible and homogeneous at the macroscopic scale. This tendency can be amplified by geometrical nanoconfinement, leading to remarkable properties. This work investigates the molecular dynamics of *tert*-Butanol (TBA)-Toluene (TOL) mixtures confined in silica nanochannels by quasielastic neutron scattering and molecular dynamics simulation. It reveals a decoupling of the molecular motion of each constituent of the binary liquid, which can be followed independently by selective isotopic HD labelling. We argue that this behavior is the signature of spatially

1
2
3 segregated dynamic heterogeneities, which are due to the recently established core-shell
4
5 nanophase separation induced by mesoporous confinement.
6
7
8
9
10
11
12
13
14
15
16
17
18
19
20
21
22
23
24
25
26
27
28
29
30
31
32
33
34
35
36
37
38
39
40
41
42
43
44
45
46
47
48
49
50
51
52
53
54
55
56
57
58
59
60

INTRODUCTION

The dynamics of nanoconfined liquids has been a topic of extensive research activities since the pioneering studies of the early 90s.¹⁻⁵ A wealth of fundamental knowledge about pure nanoconfined liquids has been collected and are subject of review articles.⁶⁻¹⁵ However, it turns out that liquid mixtures, which are particularly relevant for applications, may exhibit uncommon behaviors with respect to most studied pure systems. Fundamentally, a few studies on models systems, comprising fully miscible binary liquids confined in mesostructured porous matrices have addressed this question. The dynamics of aqueous alcohol solutions confined in MCM-41 were studied by MD simulations, dielectric spectroscopy and calorimetry experiments.¹⁶⁻¹⁸ These studies provide evidence of the possible microphase separation of fully miscible mixtures in a confined environment. More specifically, the seemingly abnormal dependence of the liquid dynamics on the concentration has been attributed to the segregation of a part of the water molecules at the pore surface, leading to an actually higher local concentration of solutes in the confined solution. As a result, two important issues emerge that are yet to be addressed experimentally: First, can direct confirmation and structural characterization of confinement-induced microphase separation be provided? Second, can one disentangle distinct dynamics that would be related to segregated molecules in the two distinct regions in the pore?

To answer the first question, we have recently reported the microphase separation of fully miscible blends of *tert*-Butanol (TBA) - Toluene (TOL) liquids confined in the cylindrical nanochannels of MCM-41 and SBA-15 mesoporous silicates (diameter $D = 3.65$ nm and 8.3 nm respectively).¹⁹⁻²² We carried out extensive structural analysis using carefully designed neutron diffraction experiments with hydrogen/deuterium isotopic substitution.^{21, 22} The measured inhomogeneous radial concentration profile demonstrates that the structure comprises a cylindrical

1
2
3 organization of two concentric core-shell regions of different compositions in which TBA
4 molecules segregate on the surface of the pores, forming an interfacial region surrounding a TOL-
5 rich core. The condition of formation of such structures was recently linked to different interfacial
6 interactions quantified experimentally by modelling the thermodynamics of binary gas
7 adsorption.²³ This observation was also confirmed by a molecular dynamics simulation study,
8 which brought a deeper insight on this phenomenon at the molecular scale.²⁴
9
10
11
12
13
14
15
16
17

18 This direct experimental evidence of the core-shell organization represents a unique insight to
19 allow the investigation of the particular dynamical properties of these novel systems. Indeed, we
20 evaluated the phase behavior and the glassy dynamics of TBA-TOL binary liquids confined in
21 MCM-41 by the combination of neutron diffraction and differential scanning calorimetry (DSC)
22 measurements in an attempt to examine the thermal behavior of this unusual phase in terms of
23 density and heat capacity.²⁵ Our studies revealed the co-existence of two different glass transitions,
24 which suggests the existence of two spatially separated dynamics, likely attributed to the
25 subcomponents of the microphase separated mixture. Although significant, this pursue to link the
26 unusual structural and dynamic properties of confined binary liquids is limited by the non-specific
27 character of calorimetry, implying that a distinction between the dynamics of the two constituents
28 has not yet been realized.
29
30
31
32
33
34
35
36
37
38
39
40
41
42
43

44 In the present study, we independently measured the dynamics of TBA and TOL molecules and
45 interpret the observed variation in light of the core-shell structure they adopt in the nanochannels.
46 In addition, we extend the investigated timescale of the dynamics from seconds (glassy dynamics
47 around T_g) to the nanoseconds (microscopic molecular motion). To achieve this objective we
48 conducted high-resolution quasi-elastic neutron scattering experiments on liquids confined in
49 SBA-15 with different isotopic compositions. Using this technique and contrast variation, the
50
51
52
53
54
55
56
57
58
59
60

1
2
3 dynamics of the hydrogenated component was highlighted due to its high incoherent cross section,
4
5 while the contribution from the complementary molecule was minimized by deuteration. The
6
7 experimental findings are discussed in the light of recent MD simulation results.
8
9

10 11 METHODS

12
13
14
15
16 **Samples.** The hydrogenated solvents TBA and TOL (>99%) were purchased from Sigma-Aldrich
17
18 and the fully deuterated solvents TBA ($C_4D_{10}O$, 99.8%) and TOL (C_7D_8 , 99.5%) were obtained
19
20 from Eurisotop and used directly, without further purification. The SBA-15 mesoporous silicates
21
22 were prepared in our laboratory using a procedure similar to that described elsewhere,^{8, 15, 26-28} with
23
24 slight modifications of the thermal treatments to optimize the final structure of the product.²⁹
25
26 Nonionic triblock copolymer (Pluronic P₁₂₃): $(EO)_{20}(PO)_{70}(EO)_{20}$ was used as a template to obtain
27
28 a mesostructured triangular array of aligned channels with a pore diameter $D = 8.3$ nm, confirmed
29
30 by nitrogen adsorption, transmission electron microscopy and neutron diffraction. The calcinated
31
32 matrix was dried at 120°C under primary vacuum for 12 hours before experiments.
33
34
35

36
37 **DSC Experiments.** For DSC measurements, SBA-15 samples were filled by liquid imbibition
38
39 with the appropriate weighted amount of fully hydrogenated TBA-TOL mixtures to allow the full
40
41 loading of the porous volume $V_P = 1 \text{ cm}^3 \text{ g}^{-1}$, as measured by nitrogen adsorption, and hermetically
42
43 sealed in aluminum pans. The measurements were performed on a TA Instrument Q20 DSC. The
44
45 thermograms were recorded at a heating rate of 10 K min^{-1} after cooling the sample from 320 K to
46
47 100 K.
48
49

50
51
52 **Quasielastic Neutron Scattering.** QENS experiments were conducted on the backscattering
53
54 instrument SPHERES operated by JCNS at the Heinz Maier-Leibnitz Zentrum (MLZ) (Garching,
55
56
57
58
59
60

Germany), at a fixed incoming wavelength of 6.27 Å, using Si (111) crystals as monochromator and analyzers.^{30,31} The resulting energy resolution is about 0.65 μeV (FWHM) and the investigated momentum transfer (Q)-range 0.16-1.8 Å⁻¹. However the analysis was limited to $Q > 0.4 \text{ Å}^{-1}$ because of contributions at lower Q values due to intense coherent scattering from the Bragg reflections of the mesoporous structure. Elastic Fixed Window Scans (EFWSs) with the monochromator Doppler drive at rest were measured during a slow heating scan at a rate of 0.75 K.min⁻¹ from about 5 K to 360 K, accumulating data points for elastic scattering over 2 minutes (i.e. $\Delta T \approx 1.5 \text{ K}$).

Sample preparation was similar for all the confined samples. A constant amount of the mesoporous materials (SBA-15) was filled into a standard flat aluminum cell for bulk and confined samples. Liquid binary mixtures (prepared in volume fraction for different isotopic and concentration compositions) were filled using a calibrated micropipette. The targeted filling was equal to 100% of the pore volume of the confinement matrix which was determined by adsorption isotherm measurements ($V_p = 1 \text{ cm}^3 \text{ g}^{-1}$). An indium wire was used to seal the sample cell. Finally, the samples were allowed to equilibrate for a few hours to ensure the homogeneous filling of the different pores, in accordance with the SANS kinetic measurements.²² In order to reduce multiple scattering, the thickness of the sample was chosen to be 1mm resulting in a transmission of typically 90% depending on the density and exact composition of the sample. Spectra were grouped, corrected for detector efficiency, empty cell and empty matrices contributions according to standard procedures using the *Slaw* software and internal routines. The corrected spectra were then normalized to the intensity measured at the lowest temperature, considering that the incoherent scattering is entirely contained in the elastic resolution under such conditions.

1
2
3 No sign of crystallization was observed in the DSC and QENS experiments, consistent with the
4 absence of bulk excess liquid outside the matrix. The pores are thus completely filled, in agreement
5 with previous studies using the same filling method.^{22, 25}
6
7

8
9
10 **Molecular Dynamics Simulations.** The simulation method is the same as used in ref. 24. A
11 silica cylindrical nanopore of diameter $D = 24 \text{ \AA}$ with a hydrophilic surface included in a cubic
12 silica cell of 35.7 \AA was obtained by applying the process proposed by Bródka and Zerda.³² We
13 generated a cylindrical cavity along the z axis of the cubic silica cell of 35.7 \AA by removing the
14 atoms within a cylinder of diameter (D) 24 \AA . From their coordination numbers, we distinguished
15 bridging oxygen (Ob) bonded to two silicon atoms from non-bridging oxygens (Onb) bonded to
16 only one silicon and bonded to one hydrogen atom (Hnb). An iterative procedure of atom (O and
17 Si) removal was applied until only tetra-coordinated silicon atoms, bonded to a maximum of two
18 Onbs, were present in the structure. Finally, non-bridging oxygens were saturated with hydrogen
19 atoms to form surface hydroxyl groups. The inner surface coverage of silanol groups was about
20 7.5 nm^{-2} . The silica matrix was subsequently kept rigid, except for the rotation around the Si-O
21 bond of the hydroxyl groups, which was allowed using the SHAKE constraints algorithm with the
22 distance between the oxygen and hydrogen atoms fixed at 1.09 \AA .
23
24
25
26
27
28
29
30
31
32
33
34
35
36
37
38
39

40 Intermolecular interactions are the sum of both electrostatic and dispersive–repulsive Lennard-
41 Jones contributions. The silica framework was modeled using the ClayFF force field.³³ The TBA
42 and TOL systems were modeled using the flexible non-polarizable OPLS force field with all atoms
43 (AA).³⁴ Whereas the intramolecular contributions (bonds, bending, and dihedral angles) were
44 conserved as original, the partial charges were calculated using ab-initio calculations. Van der
45 Waals interactions between TOL and TBA were calculated using the Lorentz-Berthelot mixing
46 rules. The LJ parameters between the silica nanopore and the TOL molecules have been optimized
47
48
49
50
51
52
53
54
55
56
57
58
59
60

1
2
3 to qualitatively reproduce the experimental isotherms.²⁴ The so-optimized interactions between
4 TOL molecules and silica material are provided in Table 1. Force field parameters of silica
5 material, TOL, and TBA and crossed interactions are provided in the FIELD.txt file of DL_POLY
6 software.³⁵
7
8
9
10
11
12

13 **Table 1.** Crossed Lennard-Jones parameters. CH₃ is the carbon of the methyl groups of toluene,
14 CH the carbon of the CH groups of toluene, and C the carbon without hydrogen atoms in toluene
15
16
17
18
19

	σ (Å)	ϵ (K)
Si-CH ₃	3.6475	46.17061
Si-CH	3.6725	47.54915
Si-C	3.6725	47.54915

20
21
22
23
24
25
26
27
28
29
30
31
32
33 The MD simulations were performed using a time step of 0.002 ps to sample 10 ns (acquisition
34 phase) with an initial configuration obtained from GCMC simulation at saturation vapor pressure
35 and at 308 K. The number of confined TBA and TOL molecules were $N_{\text{TOL}} = 84$, 64 and $N_{\text{TBA}} =$
36 98, 22 for the pure liquids and the binary mixture ($x_{\text{TBA}} = 0.24$), respectively. The equilibration
37 time corresponded to 10 ns. All MD simulations were performed with the DL_POLY package
38 using the velocity-Verlet algorithm combined with the Nose-Hoover thermostat.^{36, 37}
39
40
41
42
43
44
45
46
47

48 RESULTS AND DISCUSSION

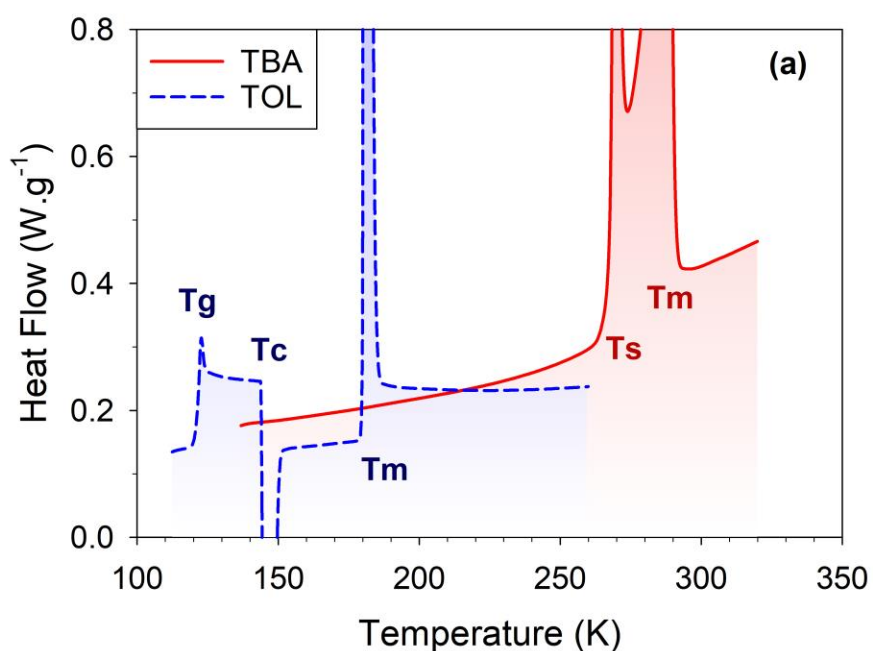
49
50
51

52 **Differential Scanning Calorimetry.** The phase behavior of the samples was determined by
53 DSC. The thermograms are shown in Figures 1a and 1b for the bulk and confined liquid
54
55
56
57
58
59
60

1
2
3 respectively. They were obtained by heating at $10 \text{ K}\cdot\text{min}^{-1}$, after a pre-cooling scan at the same
4 rate. It is well-known that under mild cooling conditions TOL generally forms a glass. The glass
5 transition is identified during heating by a jump in the heat flow, indicating an increase in heat
6 capacity, at a temperature noted T_g (121.5 K) in Figure 1a. It is followed by a sharp exothermic
7 peak at T_c (144 K) and an endothermic peak at T_m (180 K) during the subsequent heating, which
8 correspond to the cold crystallization and melting transitions, respectively. In contrast, TBA cannot
9 be vitrified, but crystallizes readily under normal cooling conditions. This behavior is confirmed
10 in Figure 1b, by the two endothermic peaks attributed, according to McGregor et al, to the
11 solid–solid transition between the trigonal $P\bar{3}$ phase (phase II) and the triclinic $P\bar{1}$ (phase IV) at T_s
12 = 268 K and the subsequent melting of the triclinic $P\bar{1}$ phase (phase IV) at $T_m = 290 \text{ K}$.³⁸
13
14
15
16
17
18
19
20
21
22
23
24
25

26 The thermograms measured for the confined systems are very different from those of the bulk,
27 as shown in Figure 1a. The first observation is the absence of exo- or endothermic peak, which
28 means that crystallization has been hindered by confinement. The pure confined liquids TOL and
29 TBA exhibit a glass transition at temperatures of $T_g^{TOL} = 118 \text{ K}$ and $T_g^{TBA} = 185 \text{ K}$, respectively.
30 For TBA, the heat capacity jump is spread over a wide temperature range (more than 20 K),
31 indicating a broadening of the distribution of relaxation times in the confined state. This probably
32 reflects the inhomogeneity of the environments experienced by the molecules located from the
33 pore surface to the center of the pore. For TOL, a tiny step around 130 K is perceived and, if real,
34 could be related to the thermal response of the interfacial layer, a phenomenon which has been
35 already observed for ortho-terphenyl confined in SBA-15.³⁹ For the binary liquid mixture, the most
36 interesting result emerges from the observation of two distinct jumps of heat capacity with
37 comparable amplitudes. These correspond to glass transitions centered around $T_g^1 = 120 \text{ K}$ and T_g^2
38 = 158 K. This result is similar to recent observations made for TBA-TOL mixtures confined in
39
40
41
42
43
44
45
46
47
48
49
50
51
52
53
54
55
56
57
58
59
60

1
2
3 MCM-41 materials (3.6 nm pore size).²⁵ They were interpreted in terms of two glass transitions
4 arising from the TOL-rich and TBA-rich phases, forming respectively the core and the shell of the
5 microphase separated liquid. It is interesting to note that the two glass transitions are sharper and
6 better resolved in the present case, which is possibly a consequence of the larger pore size of SBA-
7
8 microphase separated liquid. It is interesting to note that the two glass transitions are sharper and
9 better resolved in the present case, which is possibly a consequence of the larger pore size of SBA-
10
11 15 compared to that of MCM-41. This provided good conditions for the aimed disentangling of
12
13 core and shell contributions of the molecular dynamics of TOL and TBA molecules, as discussed
14
15 below.
16
17
18
19
20



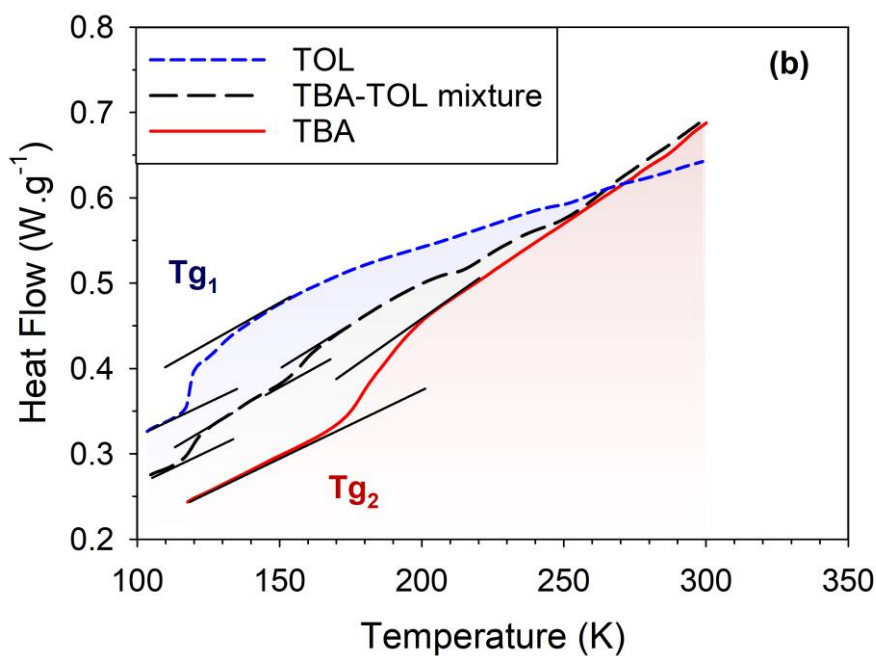


Figure 1. DSC thermograms on heating of toluene (TOL, blue dashed line) and *tert*-Butanol (TBA, red solid line) (a) in the bulk state and (b) in confinement in SBA-15. In (b), the thermogram of the TBA-TOL confined binary mixture is also added (long dashed black line). The jumps in heat capacity are underlined by thin tangential black lines just before and after each glass transition.

Elastic Fixed Window Scans. In the limit of small energy transfer, which corresponds to the quasi-elastic range, the incoherent neutron scattering function (also called dynamic structure factor) is commonly approximated by

$$S_{incoh}(Q, \omega) = e^{-\frac{\langle r^2 \rangle Q^2}{6}} [A(Q)\delta(\omega) + (1 - A(Q)) S_{quasi}(Q, \omega)] \quad (1)$$

The first term is known as the Debye-Waller factor and corresponds to the modes of vibration, where $\langle r^2 \rangle$ is the mean squared displacement (*i.e.* twice the value of $\langle u^2 \rangle$, the mean squared offset of atomic positions from their equilibrium positions), $A(Q)$ is the amplitude of the pure elastic

1
2
3 component (often noted EISF, for the Elastic Incoherent Structure Factor) describing the geometry
4
5 of localized motions and $S_{quasi}(Q, \omega)$ is the quasi-elastic component.⁴⁰
6
7

8
9 EFWS measurements are obtained by counting the elastic fraction of the dynamic structure factor
10
11 that is contained in the energy resolution of the spectrometer according to
12
13

$$I^{EFWS}(Q) = \frac{[S(Q, \omega) \otimes R(Q, \omega)](\omega=0)}{[S_{T=0}(Q, \omega) \otimes R(Q, \omega)](\omega=0)} \approx \frac{\langle S(Q, \omega) \rangle_{\Delta\omega}}{\langle S_{T=0}(Q, \omega) \rangle_{\Delta\omega}} \quad (2)$$

14
15
16
17
18 where $R(Q, \omega)$ is the resolution function of the instrument and $\Delta\omega$ is the corresponding energy
19
20 resolution width (FWHM). This quantity can be seen as the value of $S(Q, \omega)$, normalized to a zero
21
22 temperature and averaged over a narrow energy range $\Delta\omega$ (typically $\Delta\omega = 1 \mu\text{eV}$) around the elastic
23
24 peak. This equivalence would be strictly valid if the resolution function was a gate function. As a
25
26 result, EFWS give the dependence of the dynamics as a function of the temperature at the
27
28 nanosecond timescale. The EFWSs values measured for the two pure hydrogenated liquids TOL
29
30 and TBA are illustrated in Figures 2a-b.
31
32
33
34
35
36
37
38
39
40
41
42
43
44
45
46
47
48
49
50
51
52
53
54
55
56
57
58
59
60

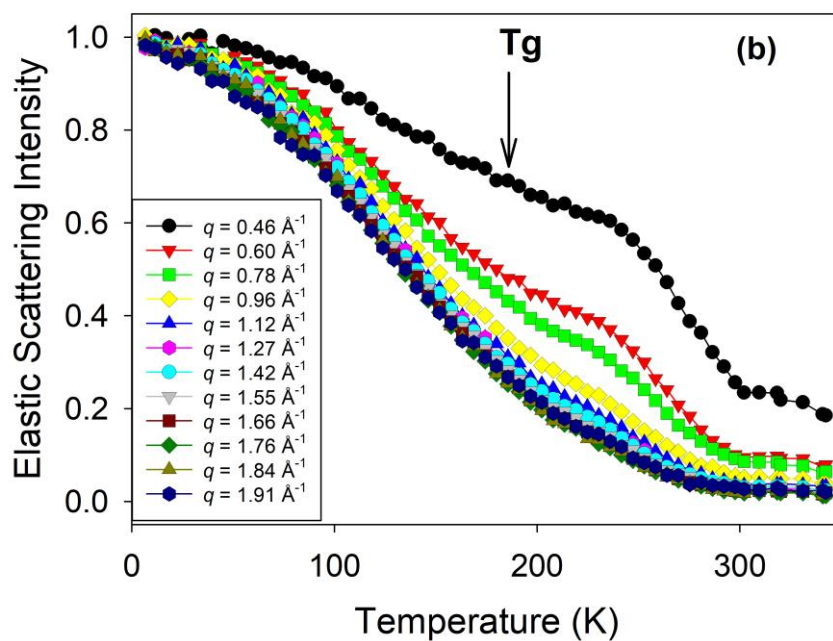
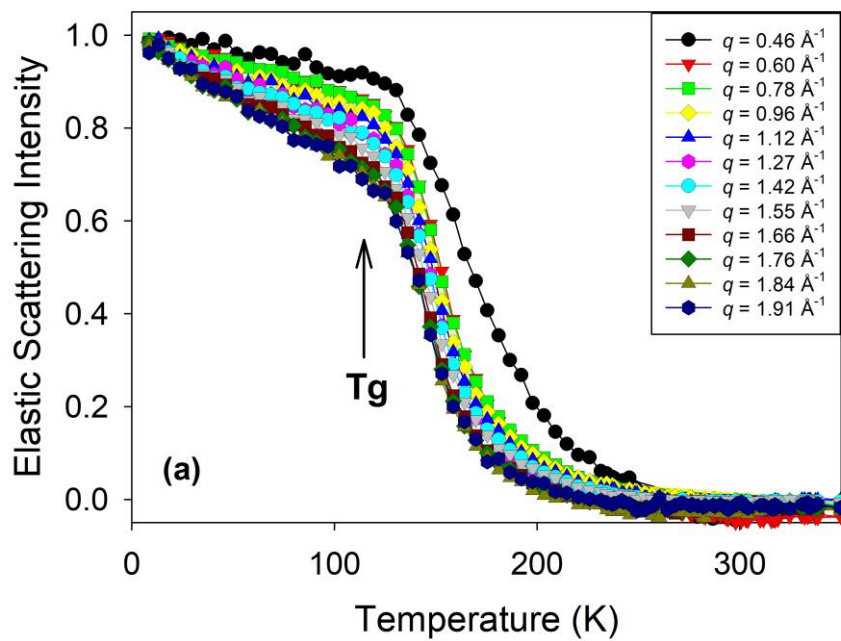


Figure 2. Elastic fixed window scans of fully hydrogenated (a) TOL and (b) TBA confined in SBA-15. The different curves correspond to different values of the momentum transfer Q ranging from 0.46 \AA^{-1} (upper curve) to 1.91 \AA^{-1} (lower curve).

For TOL, one can notice below T_g a gradual decrease of intensity during heating, which is primarily due to the Debye-Waller factor since the quasi-elastic contribution of most other modes is too slow to be distinguished from a purely elastic line. Upon further heating (above 140 K, a few tens of degrees above T_g), the intensity decreases readily to reach tiny values (< 0.1) at 200 K. This second faster decay is attributed to the onset of quasi-elastic modes (such as molecular rotation or translation), whose broadening exceeds the instrumental resolution. For TBA, there is a more pronounced decrease in the elastic intensity already at temperatures below T_g , despite its higher value compared to TOL. This indicates that the protons of TBA are already involved in fast motions (secondary modes) deep within the vitreous state. These are likely related to methyl rotations as well as tumbling and rotation of the whole molecule, favored by its globular shape.

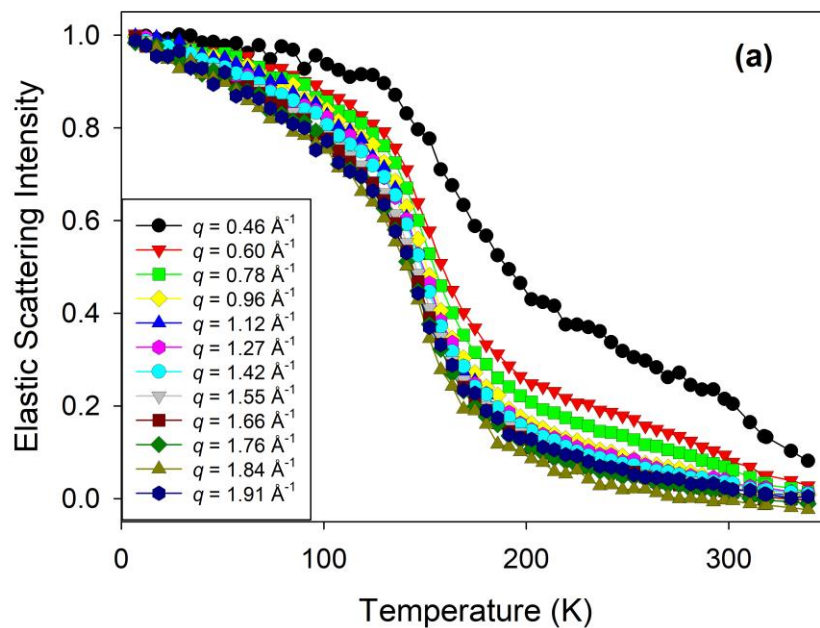
Table 2. Incoherent Scattering Cross sections of the two studied molecules as a function of their isotopic composition.

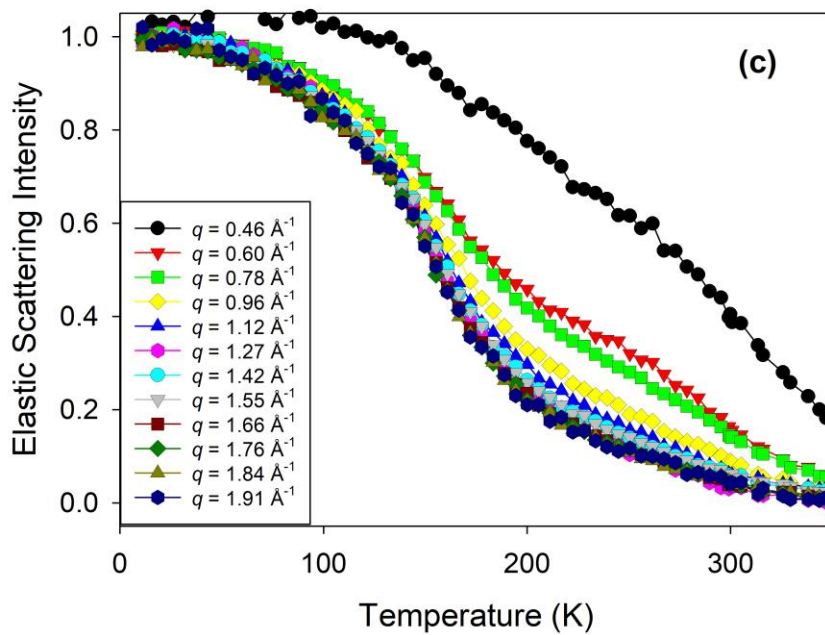
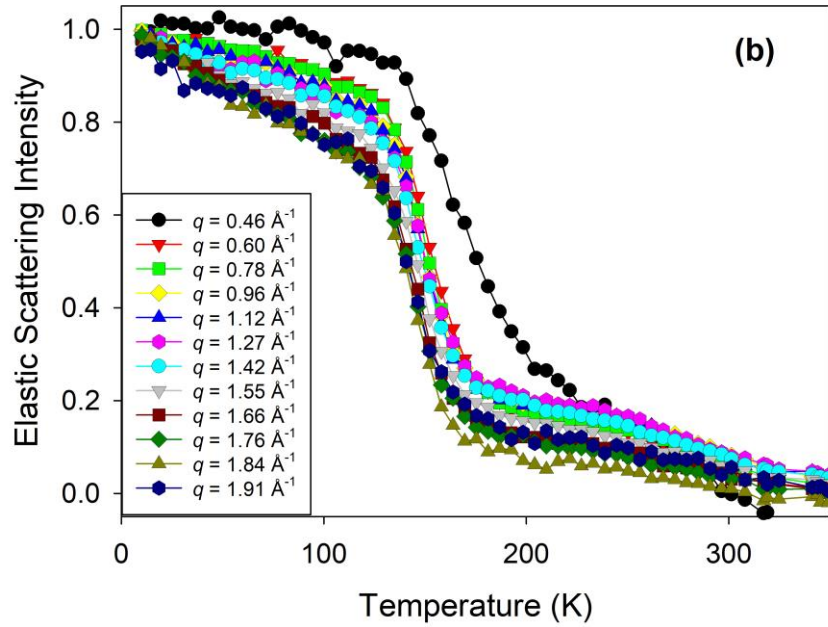
Incoherent Scattering Cross Section (10^{-24} cm^2)	TOL	TBA
Hydrogenated	639	799
Deuterated	16	20

1
2
3 We now consider the confined binary liquids for which isotopic substitution has been applied to
4 label the hydrogenated molecules and magnify their dynamics. Due to the high value of the
5 incoherent scattering cross section of hydrogen atoms, the hydrogenated molecules are expected
6 to scatter much more than their deuterated equivalents, as indicated by the molecular cross sections
7 shown in Table 2. This effect is illustrated in Figure 3 for the case of a TBA/TOL mixture with
8 equimolar composition (i.e. $x_{\text{TBA}} = 0.5$). Three different isotopic compositions were considered,
9 combining hydrogenated or deuterated molecules. They are subsequently denoted
10 TBA(H)/TOL(H), TBA(D)/TOL(H), and TBA(H)/TOL(D) mixtures.
11
12
13
14
15
16
17
18
19
20
21

22 From a comparison of Figures 3a-c, it is clear that EFWSs depend on the isotopic composition.
23 Figure 3a corresponds to the fully hydrogenated mixture TBA(H)/TOL(H), where the two
24 molecules contribute almost equally to the scattered intensity. The contribution of TOL is
25 amplified for the TBA(D)/TOL(H) sample, as shown in Figure 3b, which results in a rather marked
26 decrease in the elastic intensity above about 140 K, qualitatively resembling the case of pure TOL.
27 On the contrary, for TBA(H)/TOL(D), the decay of the elastic intensity illustrated in Figure 3c is
28 more gradual and extends to a higher temperature (i.e. above 300 K). This dependence of the elastic
29 intensity on the nature of the labelled molecule (TBA or TOL) indicates that the TBA and TOL
30 molecules undergo different dynamics in the liquid mixture. This is also consistent with the
31 observation of two previously discussed glass transition temperatures, which have been attributed
32 to the TBA-rich and TOL-rich regions, respectively. The curves presented in Figure 3d were
33 computed as the weighed sums of the EFWSs of the two pure hydrogenated systems. Their
34 similarity with the experimental EFWSs of the fully hydrogenated mixture TBA(H)/TOL(H)
35 further support that the elastic intensity of the mixture actually results from the coexistence of two
36
37
38
39
40
41
42
43
44
45
46
47
48
49
50
51
52
53
54
55
56
57
58
59
60

1
2
3 distinct dynamical contributions, arising respectively from spatially segregated TBA-rich and
4
5 TOL-rich regions.
6
7
8
9
10
11
12
13





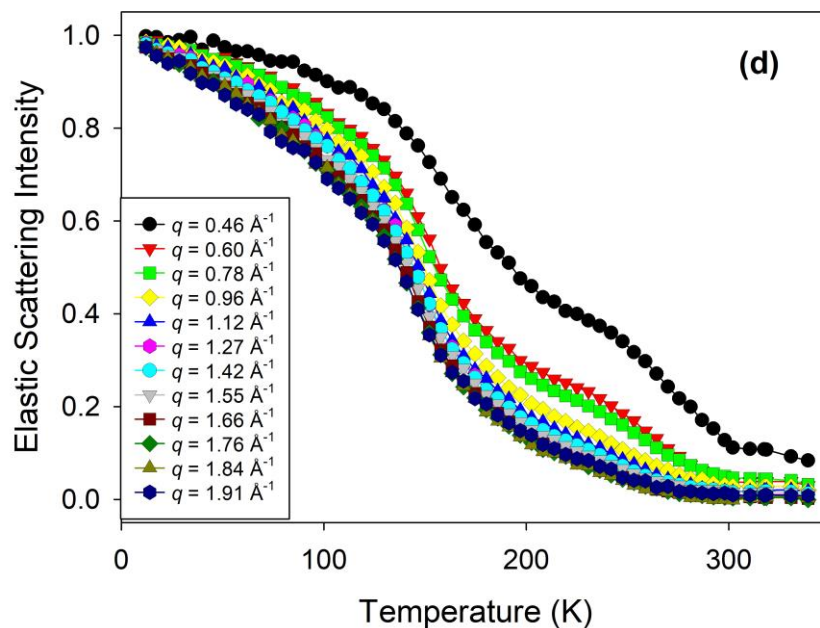


Figure 3. Elastic fixed window scans of the TBA/TOL binary mixtures confined in SBA-15 with a molar fraction of TBA $x = 0.5$. Keeping the same chemical composition, the mixtures differ in their isotopic composition with (a) TBA(H)/TOL(H), (b) TBA(D)/TOL(H) and (c) TBA(H)/TOL(D). (d) The linear combination of the elastic fixed window scans of the two pure fully hydrogenated liquids for comparison with the actual equimolar mixture (a).

From the Q -dependence of the EFWS one can derive the Mean Square Displacement (MSD), which is a complementary way to study the dynamic structure factor.⁴⁰⁻⁴² At low temperatures, the quasi-elastic lines related to relaxation processes are sufficiently narrow with respect to the experimental resolution and cannot be distinguished from a true elastic peak. Therefore, setting $S_{quasi}(Q, \omega) = \delta(\omega)$ in Eq.1, it becomes:

$$I^{EFWS}(Q) \propto e^{-\frac{\langle r^2 \rangle Q^2}{6}} \quad (3).$$

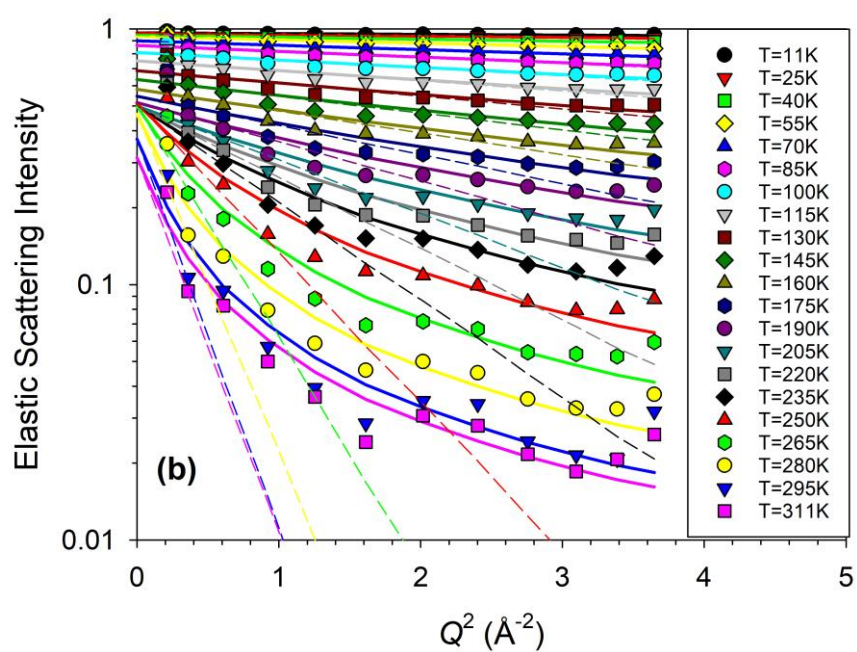
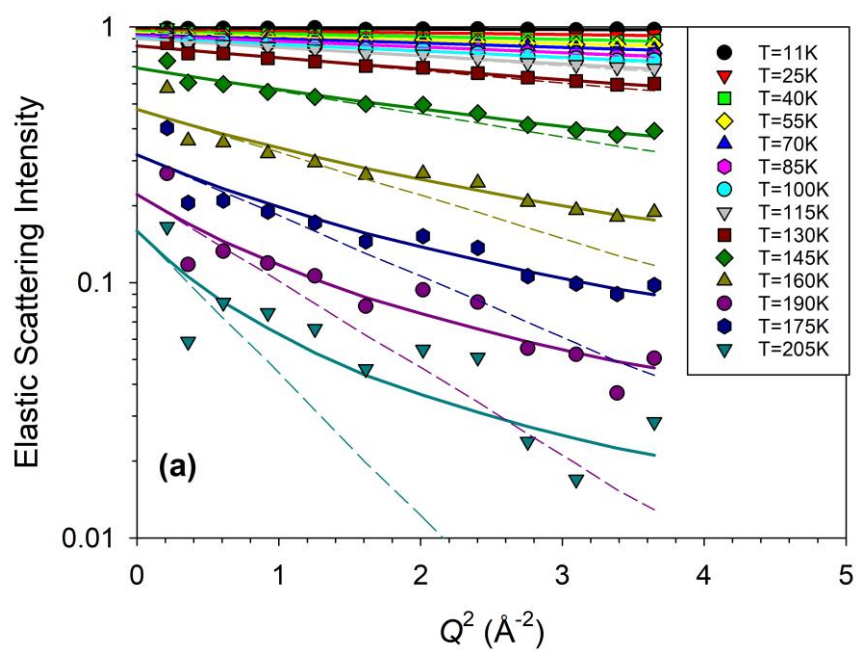
The most common procedure used to extract the MSD consists in performing a linear fit of Q^2 versus $\ln(I^{EFWS}(Q))$, where $\langle r^2 \rangle$ is simply deduced from the slope. This analysis is presented in Figures 4a-b for confined TOL and TBA, for a selection of temperatures. It is well-known that this Gaussian law is valid for purely vibrational modes, a situation which is often encountered at low temperature, but deviations are generally observed at increasing temperatures. In our study, one notes that this approximation works well up to about 150 K, as shown in Figures 4a-b. At higher temperature, there is a marked curvature, due to anharmonic effects and the onset of quasi-elastic processes. In addition, the extrapolation of EFWS to $Q = 0$ deviates from unity, a phenomenon that can be enhanced by multiple scattering.

Zorn has shown that EFWSs could still be modelled at a higher temperature if the diffusion processes were taken into account.⁴³ In this case, the definition of the MSD is extended beyond the simple harmonic case by

$$I^{EFWS}(Q) \propto \operatorname{erfcx}\left(\frac{-\sqrt{\pi}\langle r^2 \rangle Q^2}{2} \frac{1}{6}\right) \quad (4)$$

where erfcx is the scaled complementary error function, defined by $\operatorname{erfcx}(X) = \exp(X^2)(1 - \operatorname{erf}(X)) = \frac{2}{\sqrt{\pi}} \exp(X^2) \int_X^\infty \exp(-t^2) dt$.

Note that in the limit of $\langle r^2 \rangle Q^2 \rightarrow 0$, which is applicable at low temperature, this generalized definition of $I^{EFWS}(Q)$ given by Eq. 4 becomes equivalent to the common Gaussian approximation given by Eq. 3.



1
2
3 **Figure 4.** Elastic fixed window scans of (a) TOL and (b) TBA confined in SBA-15 at different
4 temperatures. The log-scale of EFWS intensity plotted as a function of the squared momentum
5 transfer emphasizes the temperature range where the usual Gaussian approximation applies
6 (typically for $T < 150$ K). Fits with the generalized model (solid line) and its low- Q Gaussian
7 approximation (dashed line) are shown. For better clarity, the data shown here are averaged values
8 over 10 successive measurements, so that the temperature step is about 15 K.
9

10
11
12
13
14
15
16
17
18 Fit curves using this generalized approach are represented by solid lines in Figures 4a-b. Gaussian
19 extrapolations of Eq. 4 to zero Q are also indicated by dashed lines. Although the first allowed
20 better adjustments at temperatures above about 150 K, we selected the MSDs derived from the
21 latter procedure to evidence a trend. In what follows, we draw conclusions exclusively from the
22 low temperature range, where the Gaussian approximation is indeed valid and where the intensity
23 of the EFWS is still high (greater than 0.5), assuming that the conditions necessary to ignore
24 secondary contributions to EFWS, such as the coherent scattering and scattering of unlabeled
25 molecules, are met.
26
27
28
29
30
31
32
33
34
35
36

37 **Mean Squared Displacement - Experiments.** The dynamics of the H-labeled TOL molecules
38 derived from neutron backscattering experiments is illustrated in Figure 5 for different
39 compositions of the binary mixture. Isotopically labeled mixtures of TBA(D)-TOL(H) were used
40 in order to emphasize the mean squared displacement of the H-tagged TOL molecules and to
41 evaluate the effect of the addition of TBA ($x_{\text{TBA}} = 0, 0.3, 0.5, \text{ and } 0.7$) on the dynamics of TOL.
42
43
44
45
46
47
48
49

50 The MSDs increase almost linearly with the temperature up to about 130 K, where they show a
51 strong increase. The behavior observed in the low temperature region is typical for the vibrational
52 dynamics of solid (glassy) systems and is consistent with the Debye harmonic approximation. The
53
54
55
56
57
58
59
60

1
2
3 steep increase above 130 K indicates the onset of local modes with larger amplitudes including
4 librations of molecules and rattling in the neighbor's cage. An influence of the increasing TBA
5 content on the TOLH-MSD could not be determined within the experimental uncertainties, except
6 for the highest TBA fraction at which a small effect is observed above 130 K, as discussed below.
7
8 Larger mixing effects could have been expected, given that TBA is more viscous than TOL and
9 could have acted as a slowing additive. We infer that this can be rationalized by the concomitance
10 of three facts: first, the core-shell structure adopted by the TBA-TOL mixtures in confinement
11 limits the molecular mixing, so that the TOL environment is maintained in the TOL-rich core
12 region despite dilution. Secondly, the measured MSDs reflect the local dynamics, which is in fact
13 mostly sensitive to the short-ranged environment. Finally, interfacial effects (such as TOL-TBA
14 or TOL-Silica interactions) are presumably low for TOL due to its Van-der-Waals character.
15 Consistently, small BET constants were deduced from the adsorption isotherm experiments of
16 TOL in porous silica.²³

17
18
19 To conclude the discussion of Figure 5, the observed weaker increase of the TOL MSD near 130
20 K for $x_{\text{TBA}} = 0.7$ compared to the other three compositions is particularly interesting. Indeed, this
21 suggests that the addition of TBA eventually slows down the dynamics of TOL, at least in the 130-
22 150 K region where the aforementioned precautions concerning the uncertainties of MSDs are
23 properly accounted for. According to the DSC study, this region is located well below the glass
24 transition of TBA. Therefore, we deduce that the reduced large amplitude motions observed for
25 $x_{\text{TBA}} = 0.7$ near 130 K might be a signature of TOL molecules trapped in TBA-rich glassy
26 microdomains. The fact that smaller displacements of TOL are seen only for the largest fraction
27 of TBA, i.e. corresponding to the strongest confinement condition when considering the TBA

surface layer, agrees well with previous observations for pure confined TOL, which indicated that pore diameters as small as 2.4 nm were necessary to significantly affect its glassy dynamics.⁷

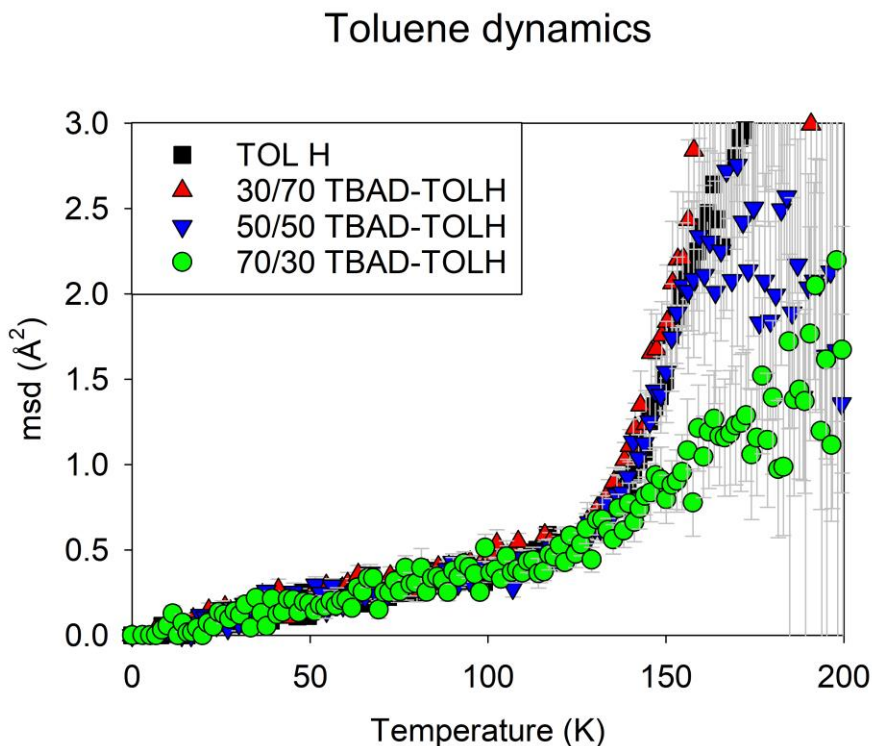
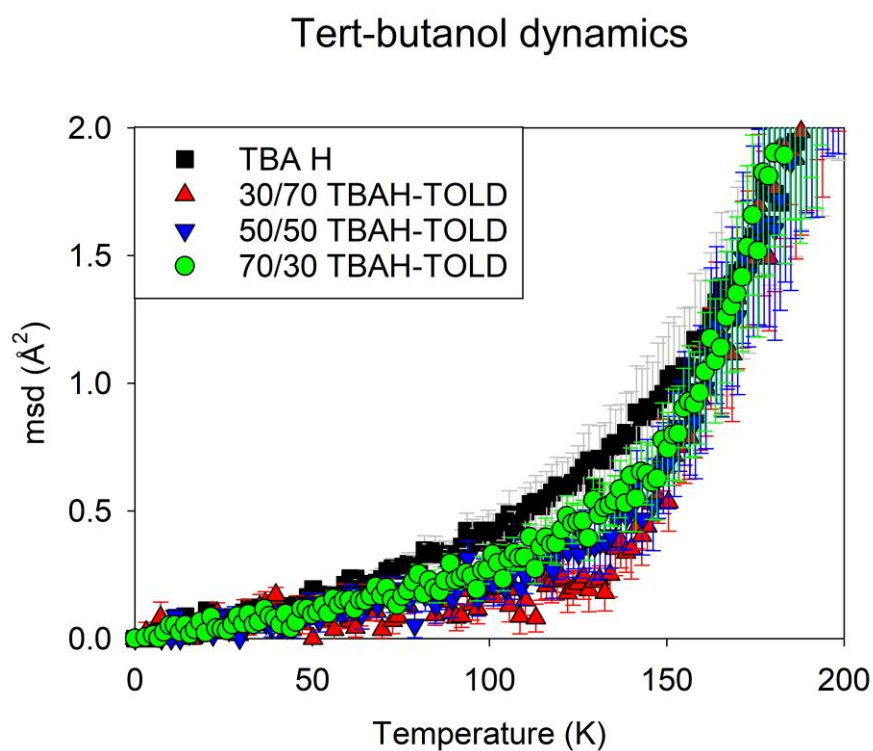


Figure 5. Mean squared displacement of TOL H-tagged-molecules, derived from neutron backscattering experiments on confined TBA(D)-TOL(H) binary mixtures with different compositions (TBA molar fractions $x = 0, 0.3, 0.5,$ and 0.7). The MSD is the result of an analysis with the low Q approximation (see text).

We look now on the opposite labeling, the MSDs of H-tagged TBA molecules confined in SBA-15, which are illustrated in Figure 6. A systematic decrease in MSDs as a function of TOL content is observed in the temperature range of 100 to 150 K. This dependence can be considered as a perfect illustration of the unusual physical behavior of microphase-separated binary fluids because it contradicts interpretations based on simple mixing effects. TOL is a non H-bonding solvent with

1
2
3 a lower viscosity than the H-bonding TBA. According to the usual dilution effects, we could have
4 expected a reduction of the H-bond interactions between the TBA molecules, as shown for bulk
5 mixtures of TBA-TOL,⁴⁴ resulting in faster TBA dynamics, as reported for other alcohol-alkane
6 mixtures (Br-butane-butanol mixtures) by NMR and MD simulation.⁴⁵ However, this apparently
7 anomalous dilution effect can be easily rationalized by taking the core-shell microstructure of
8 confined TBA-TOL mixtures into account.
9
10
11
12
13
14
15



43
44
45
46
47
48
49
50
51
52
53
54
55
56
57
58
59
60

Figure 6. Mean squared displacement of TBA H-tagged-molecules, derived from neutron backscattering experiments for TBA(H)-TOL(D) confined binary mixtures with different compositions (TBA molar fractions $x = 1, 0.7, 0.5,$ and 0.3).

1
2
3 The interpretation is illustrated in Figure 7, where the core-shell structure of TBA-TOL binary
4 mixtures is depicted. It is usually observed that the dynamics of nanoconfined liquids are
5 heterogeneous.⁴⁶⁻⁴⁹ This fact could be related to the increase in the stretched character of the
6 relaxation function,^{50, 51} or equivalently to the temperature broadening (sometimes bimodal) of the
7 glass transition.^{7, 39} Dynamic heterogeneities can be related to a wide relaxation times distribution
8 $g(\tau)$, as shown in Figure 7a. While dynamic heterogeneities in supercooled liquids are often
9 described as the coexistence of slow and fast dynamically distinct domains, their spatial nature is
10 more clearly established under confinement. Indeed, surface interactions mostly slow down the
11 mobility of interfacial molecules. The effect of this boundary condition can propagate towards the
12 pore center up to a few molecular sizes.^{13, 50, 52, 53} It can be expected that bulk-like behaviors are
13 recovered sufficiently far from the pore surface. Depending on the ratio between the characteristic
14 length of the interfacial layer and the pore size, a gradient scenario or a two-layers (two- T_g s)
15 scenario can be preferred.¹³ The resulting radial distribution of mobility is illustrated in Figure 7b,
16 where the darker the region, the slower its dynamics. The corresponding time τ_{TBA} is plotted in
17 solid white line. In the temperature range 0-200 K, the MSDs measured experimentally are smaller
18 than 3 \AA^2 , which is negligible compared to the squared pore size ($D^2 = 7\ 000 \text{ \AA}^2$). It means that
19 each molecule remains essentially in the same environment on the studied timescale and its MSD
20 reflects the local dynamics. A spatial average results from averaging over molecules which are
21 located at different places in the pore. For pure TBA, the measured EFWS is spatially averaged
22 over the entire pore volume, including both the slower interfacial region and the faster pore center
23 region. In this case a direct experimental disentanglement of both contributions is hardly possible,
24 whereas it is simple by molecular simulation.^{52, 54-57} However, as is illustrated by Figures 7c-d,
25 we demonstrate here that the H-labeling of the TBA molecules makes it possible to highlight the
26
27
28
29
30
31
32
33
34
35
36
37
38
39
40
41
42
43
44
45
46
47
48
49
50
51
52
53
54
55
56
57
58
59
60

dynamics of the surface molecules of the core-shell structure which is adopted during the addition of TOL. As a result, the EFWSs measured for TBA(H)/TOL(D) mixtures with an increasing fraction of TOL are particularly sensitive to the slowest part of the relaxation time distribution $g(\tau)$, as sketched in Figure 7a. This also rationalizes the apparently counterintuitive “anti-plasticizing effect” of TOL on TBA dynamics.

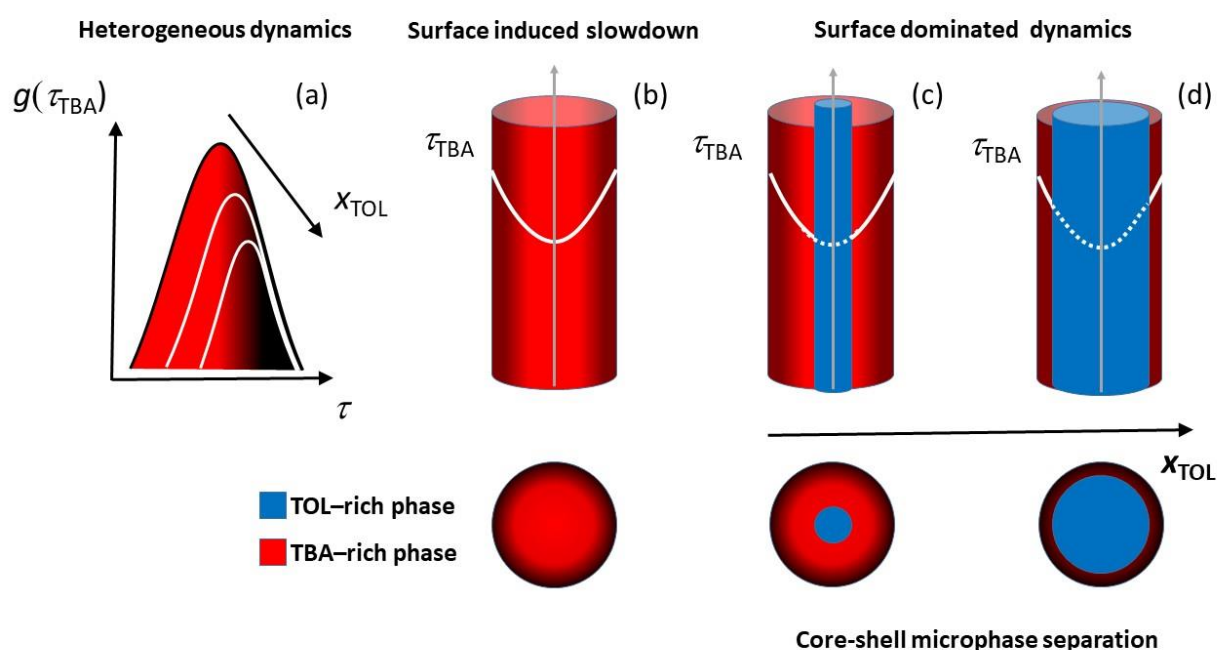


Figure 7. Schematic illustrations of (a) the variation of the relaxation times distribution $g(\tau)$ and (b-d) the dynamical heterogeneities formed by the TBA-rich (in red) and TOL-rich (blue) regions inside a cylindrical nanopore as a function of the volume fraction TOL x_{TOL} . Slower (interfacial) regions are identified by a darker red color.

Mean Squared Displacement – MD Simulation. A molecular simulation study was conducted in order to underline our interpretation of the quasi-elastic neutron scattering experiments. It is based

1
2
3 on a recently published model, capable of reproducing the microphase separation of TBA-TOL
4
5 mixtures, experimentally demonstrated when confined in silica pore $D = 2.4$ nm.²⁴ The simulation
6
7 was performed at a temperature ($T = 308$ K) significantly higher than that of the experiments in
8
9 order to guarantee equilibration. Although it prevents us from making a direct quantitative
10
11 comparison, it allows us to identify the salient features discovered experimentally and to provide
12
13 them with a microscopic point of view.
14
15

16
17
18 The radial density profile of the pure TBA exhibits layering as a function of the distance r from
19
20 the pore center (cf. Figure 8a), which is a common feature of confined liquids reported by
21
22 molecular simulation studies.^{56, 58} The spatially heterogeneous distribution of molecules was used
23
24 to distinguish the interfacial layer ($8 < r < 12$ Å) and the central region ($0 < r < 8$ Å). The MSDs
25
26 of TBA computed for these two regions are illustrated in Figure 8b. The mobility of the interfacial
27
28 TBA molecules is significantly reduced with respect to the core region, as indicated by an MSD
29
30 variation of about a factor ten. This observation is consistent with the schematic illustration of
31
32 Figure 7a. It emphasizes the role of surface interaction, and in particular the formation of H-bonds
33
34 with surface silanols, on the heterogeneous nature of the dynamics of the confined liquid.
35
36
37
38
39
40
41
42
43
44
45
46
47
48
49
50
51
52
53
54
55
56
57
58
59
60

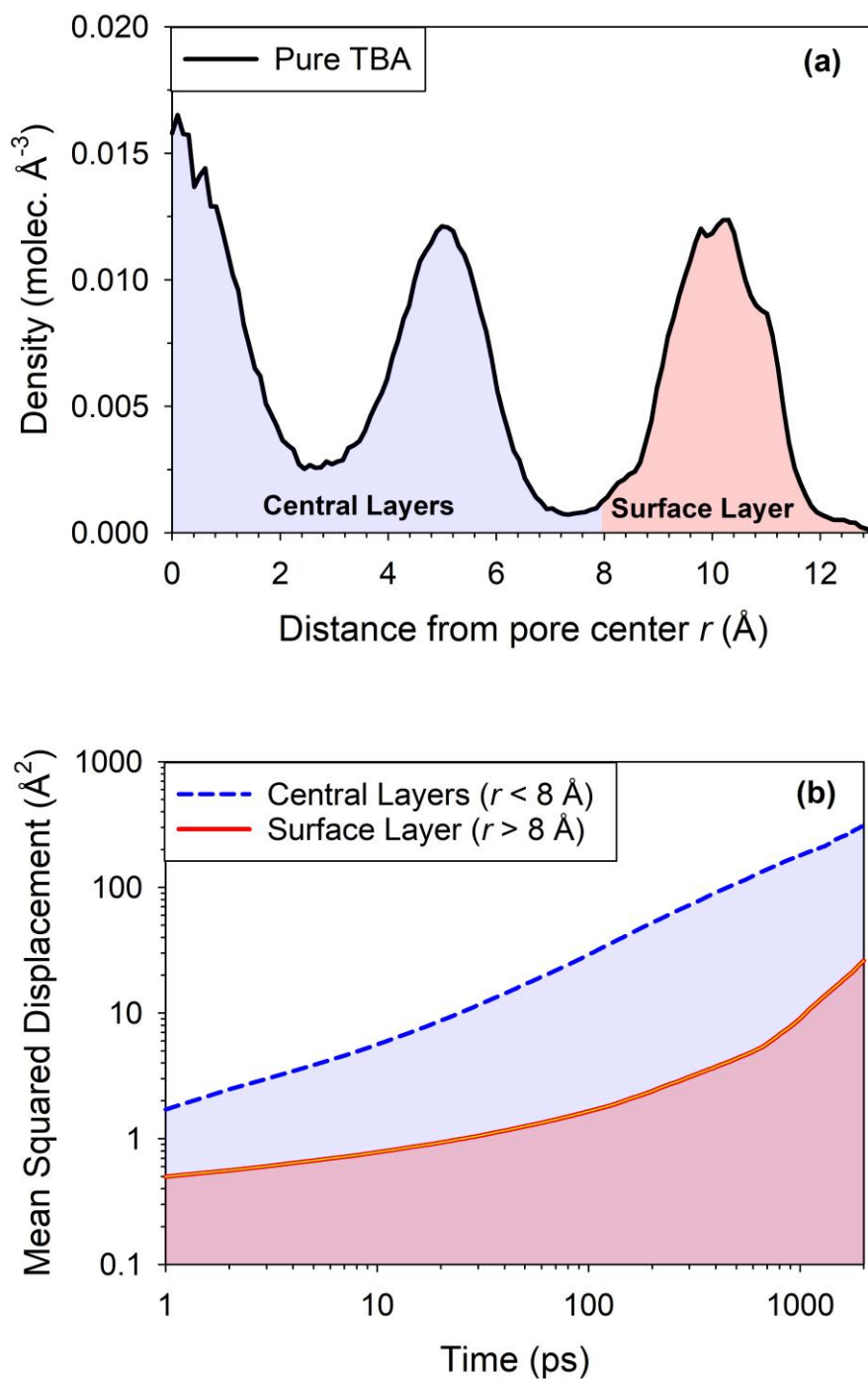
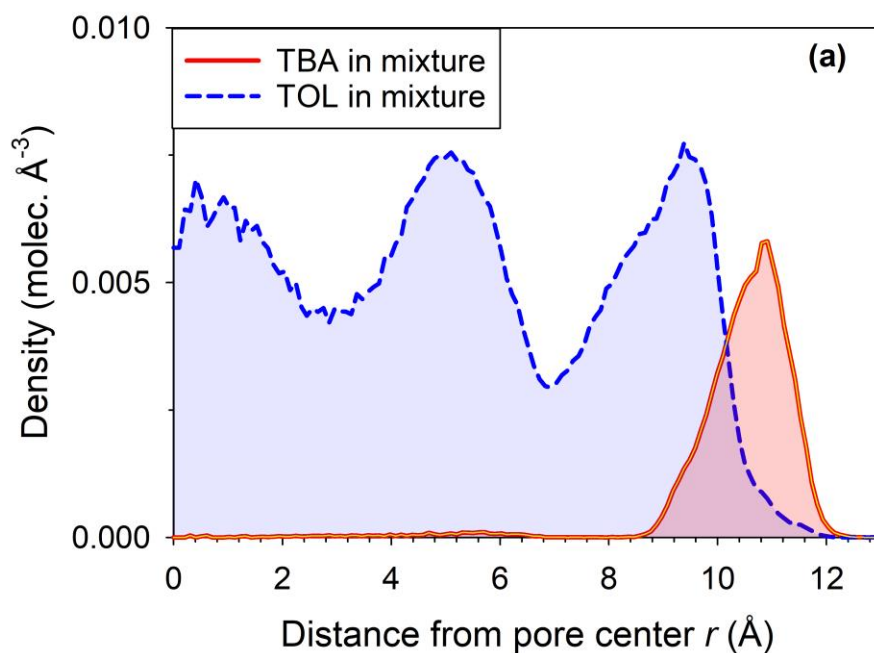


Figure 8. (a) Radial density profile of the center of mass of pure TBA confined in nanoporous silica at 308 K, and (b) MSD of TBA molecules as a function of their distance from the pore center, dashed line : pore center region ($0 < r < 8$ Å), solid line : surface layer : ($8 < r < 12$ Å).

1
2
3
4
5
6
7 The structure adopted by the binary mixture ($x_{\text{TBA}} = 0.24$) is illustrated in Figure 9a by the radial
8 density profiles of the two molecules. Segregation of the two components is observed, leading to
9 a core-shell structure where the TBA molecules are preferentially located at the pore surface and
10 TOL at the center of the pore. This microphase separation is driven by the different strength of the
11 liquid-surface interactions of TBA and TOL molecules, as indicated in previous studies.
12
13
14
15
16
17
18
19
20



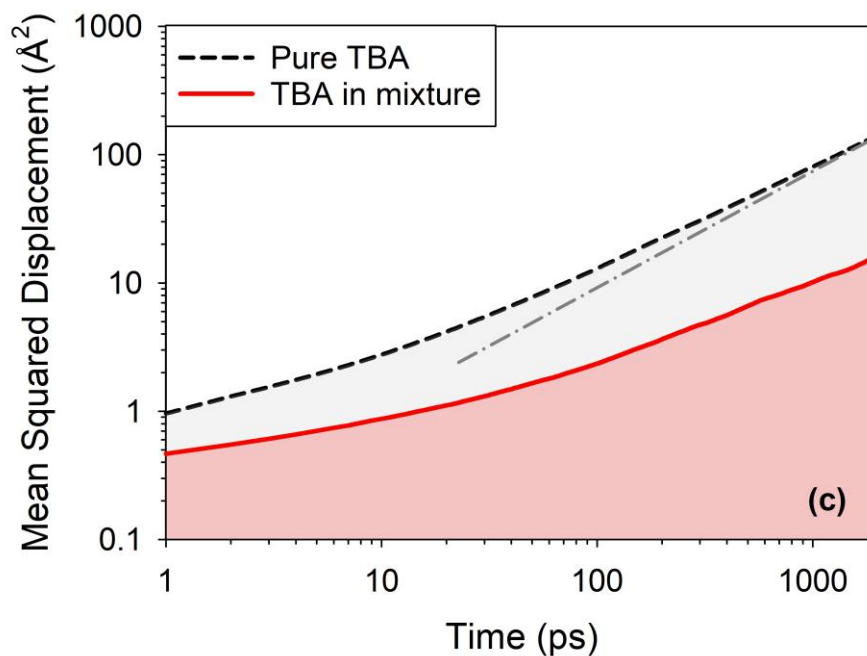
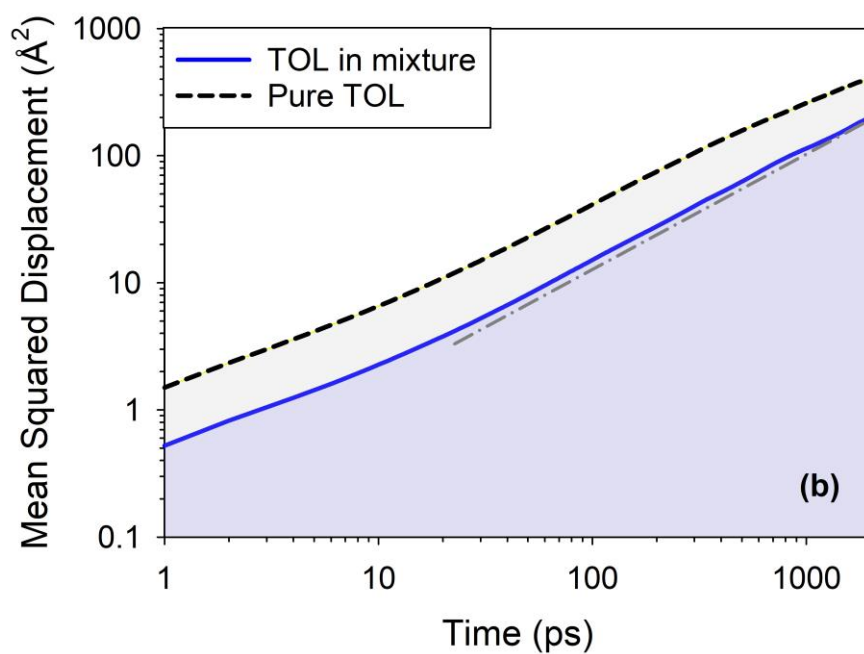


Figure 9. (a) Radial density profile of the center of mass of TBA (solid line) and TOL (dashed line) molecules in the confined binary mixture ($x_{\text{TBA}} = 0.24$). (b) MSD of TOL molecules in the

1
2
3 pure (dashed line) and in the binary mixture (solid line), and (c) MSD of TBA molecules in the
4
5 pure (dashed line) and in the binary mixture (solid line). The dashed-dotted line is a guideline with
6
7 a linear slope corresponding to the diffusive behavior.
8
9

10
11 The time dependent MSDs of the TOL and TBA molecules are illustrated in Figures 9b and c,
12
13 respectively. These are simulated counterparts of experimental the EFWS (corresponding to
14
15 several nanoseconds) with H-labeled molecules. The dynamics of TOL in pure and binary liquids
16
17 are qualitatively similar. Specifically, the MSDs of both samples present a linear dependence on
18
19 time (indicated by a dashed-dotted line), which indicates the normal Fick diffusion law. Slightly
20
21 slower dynamics are witnessed for the mixture, which is demonstrated by a reduction in the MSD
22
23 by a factor of two. This suggests that, due to the microsegregation phenomenon, the local
24
25 environment of the TOL molecules is maintained in the binary liquid, and thus its dynamics are
26
27 weakly affected. This is in agreement with the experiments discussed above. A slight deceleration
28
29 may indicate a weak coupling of the TOL mobility with the slower dynamics of TBA, but this
30
31 could also originate from the stronger effective confinement imposed by the non-moving shell on
32
33 the liquid core. It is interesting to note that the dynamics of the TBA varies considerably with the
34
35 addition of TOL, as shown in Figure 9c, where the MSD is reduced by one order of magnitude.
36
37 Moreover, the TBA dynamics exhibit a clear sub-diffusive character in the confined mixture, while
38
39 obeying a Fick law in the pure liquid form. It should be emphasized again that this behavior is in
40
41 contradiction with the simple mixing effect (plasticizing) of TOL on TBA. In fact, the MSDs of
42
43 TBA in the mixture demonstrate values similar to those of the contact layer in the pure component.
44
45 This supports our understanding that the unexpected dynamics of TBA is closely related to the
46
47 core-shell structure adopted by binary liquids under confinement.
48
49
50
51
52
53
54
55
56
57
58
59
60

CONCLUSIONS

The dynamics of binary liquids confined in the straight and monodispersed channels of ordered SBA-15 mesoporous materials were investigated by elastic fixed window scans to probe nanosecond timescales. Pure components as well as different binary mixtures were studied in which selective isotopic labeling was used to highlight the dynamics of the hydrogenated component. Mean squared displacements were acquired from the Q -dependence of the EFWS scans, and their interpretation was substantiated by the results of MD simulation.

According to the experiments carried out on the various TBA(D)/TOL(H) mixtures, it appears that the dynamics of TOL does not vary significantly with the addition of TBA. This behavior corroborates the poor mixing of both components in confined geometry, as also indicated by the observation of two distinct glass transitions and previously published structural studies. Furthermore, the experiments on the various TBA(H)/TOL(D) mixtures indicate a reduction of the MSDs of TBA when the fraction of TOL increases. Since TOL is a non-H-bonded additive with a glass transition temperature much lower than that of TBA, this observed impact on TBA dynamics cannot be understood by simple mixing rules. On the contrary, we propose a simple rationalization of this counterintuitive behavior based on the microscopic pictures provided by MD simulation, and by taking into account the specific nature of nanoconfined binary liquids and their recently discovered tendency to form core-shell microphase separated structures.²² For the pure liquid, the measured mobility of TBA reflects a spatial average on dynamic heterogeneities ranging from the center of the pore to the pore wall, whereas for the binary systems, the core-shell structure makes it specifically representative of the interfacial molecules of TBA. Due to the strong interaction between silica and TBA molecules induced by the formation of H-bonds, it is logical that the

1
2
3 dynamics of interfacial molecules probed for TBAH/TOLD mixtures represent the slowest tail of
4
5 the relaxation times distribution of the confined liquid.
6
7

8
9 These findings verify and confirm from a dynamic point of view the structure proposed by
10 the modeling of small angle neutron scattering data.²² To our knowledge, this combination of direct
11 experimental studies on confinement-induced microphase separated liquids both from a structural
12 and a dynamic point of view is rather unique in literature. We therefore expect that this approach
13 will help to better understand other cases discussed in the literature in which dynamic evidences
14 of microphase demixing are reported.^{16-18, 59, 60}
15
16
17
18
19
20
21
22

23 It is worth noting that this study gives a clearer insight on the nature of the dynamic
24 heterogeneities, which have also been observed for the same liquids confined in the smaller pores
25 of MCM-41 materials by calorimetry.²⁵ Beyond those calorimetric results, the interpretation of
26 which being limited by the absence of chemical selectivity of DSC, the significance of this study
27 lies in its ability to make a real distinction between the dynamics of the two molecular components
28 (TBA and TOL molecules) constituting the confined binary mixtures. In addition to MD
29 simulation, one cannot ignore the exceptional value of neutron scattering methods with
30 component-selective H/D labeling in providing a direct correlation between spatially segregated
31 dynamical heterogeneities and the formation of original core-shell nanostructures. These critical
32 findings call for further investigations. Beyond the need to extent the study to different systems
33 and timescale, a subsequent quantitative dynamic analysis remains essential for a full insight on
34 the physical behavior of such complex systems under confinement.
35
36
37
38
39
40
41
42
43
44
45
46
47
48
49
50
51
52
53
54
55
56
57
58
59
60

ACKNOWLEDGMENTS

The experiments were performed in the frame of the PhD project of R. Mhanna who acknowledges funding by the Institute Laue-Langevin and the Brittany Region (ARED 7784 / NanoBina). Support from Europe (FEDER) and Rennes Metropole is expressly acknowledged. This project has received funding from the European Union's 7th Framework Programme for research, technological development and demonstration under the NMI3-II Grant number 283883. We thank Odile MERDRIGNAC (Institut des Sciences Chimiques de Rennes) for her assistance with Nitrogen isotherms experiments for the characterization of the SBA-15 materials.

REFERENCES:

1. Jackson, C.; McKenna, G., The Glass-Transition of Organic Liquids Confined to Small Pores. *Journal of Non-Crystalline Solids* **1991**, *131*, 221-224.
2. Granick, S., Motions and Relaxations of Confined Liquids. *Science* **1991**, *253* (5026), 1374-1379.
3. Zhang, J.; Liu, G.; Jonas, J., Effects of Confinement on the Glass-Transition Temperature of Molecular Liquids. *Journal of Physical Chemistry* **1992**, *96* (8), 3478-3480.
4. Arndt, M.; Stannarius, R.; Gorbatschow, W.; Kremer, F., Dielectric Investigations of the Dynamic Glass Transition in Nanopores. *Physical Review E* **1996**, *54* (5), 5377-5390.
5. Schuller, J.; Melnichenko, Y.; Richert, R.; Fischer, E., Dielectric Studies of the Glass Transition in Porous Media. *Physical Review Letters* **1994**, *73* (16), 2224-2227.
6. Christenson, H. K., Confinement Effects on Freezing and Melting. *Journal of Physics-Condensed Matter* **2001**, *13* (11), R95-R133.
7. Morineau, D.; Xia, Y. D.; Alba-Simionesco, C., Finite-Size and Surface Effects on the Glass Transition of Liquid Toluene Confined in Cylindrical Mesopores. *Journal of Chemical Physics* **2002**, *117* (19), 8966-8972.
8. Alba-Simionesco, C.; Dosseh, G.; Dumont, E.; Frick, B.; Geil, B.; Morineau, D.; Teboul, V.; Xia, Y., Confinement of Molecular Liquids: Consequences on Thermodynamic, Static and Dynamical Properties of Benzene and Toluene. *European Physical Journal E* **2003**, *12* (1), 19-28.

- 1
2
3 9. Morineau, D.; Alba-Simionesco, C., Liquids in Confined Geometry: How to Connect
4 Changes in the Structure Factor to Modifications of Local Order. *Journal of Chemical Physics*
5 **2003**, *118* (20), 9389-9400.
6
7
8
9
10 10. Alcoutlabi, M.; McKenna, G. B., Effects of Confinement on Material Behaviour at the
11 Nanometre Size Scale. *Journal of Physics-Condensed Matter* **2005**, *17* (15), R461-R524.
12
13
14 11. Alba-Simionesco, C.; Coasne, B.; Dosseh, G.; Dudziak, G.; Gubbins, K. E.;
15 Radhakrishnan, R.; Sliwinska-Bartkowiak, M., Effects of Confinement on Freezing and Melting.
16 *Journal of Physics-Condensed Matter* **2006**, *18* (6), R15-R68.
17
18
19
20 12. Morineau, D.; Alba-Simionesco, C., Does Molecular Self-Association Survive in
21 Nanochannels? *Journal of Physical Chemistry Letters* **2010**, *1* (7), 1155-1159.
22
23
24
25 13. Richert, R., Dynamics of Nanoconfined Supercooled Liquids. *Annual Review of Physical*
26 *Chemistry, Vol 62* **2011**, *62*, 65-84.
27
28
29
30 14. Huber, P., Soft Matter in Hard Confinement: Phase Transition Thermodynamics,
31 Structure, Texture, Diffusion and Flow in Nanoporous Media. *Journal of Physics-Condensed*
32 *Matter* **2015**, *27* (10).
33
34
35
36 15. Audonnet, F.; Brodie-Linder, N.; Morineau, D.; Frick, B.; Alba-Simionesco, C., From
37 the Capillary Condensation to the Glass Transition of a Confined Molecular Liquid: Case of
38 Toluene. *Journal of Non-Crystalline Solids* **2015**, *407*, 262-269.
39
40
41
42
43 16. Elamin, K.; Jansson, H.; Kittaka, S.; Swenson, J., Different Behavior of Water in
44 Confined Solutions of High and Low Solute Concentrations. *Physical Chemistry Chemical*
45 *Physics* **2013**, *15* (42), 18437-18444.
46
47
48
49
50
51
52
53
54
55
56
57
58
59
60

- 1
2
3 17. Swenson, J.; Elamin, K.; Chen, G.; Lohstroh, W.; Sakai, V. G., Anomalous Dynamics
4 of Aqueous Solutions of di-Propylene Glycol Methylether Confined in MCM-41 by Quasielastic
5 Neutron Scattering. *Journal of Chemical Physics* **2014**, *141* (21).
6
7
8
9
10 18. Elamin, K.; Jansson, H.; Swenson, J., Dynamics of Aqueous Binary Glass-Formers
11 Confined in MCM-41. *Physical Chemistry Chemical Physics* **2015**, *17* (19), 12978-12987.
12
13
14 19. Hamid, A.; Lefort, R.; Lechaux, Y.; Moreac, A.; Ghoufi, A.; Alba-Simionesco, C.;
15 Morineau, D., Solvation Effects on Self-Association and Segregation Processes in tert-Butanol-
16 Aprotic Solvent Binary Mixtures. *Journal of Physical Chemistry B* **2013**, *117* (35), 10221-10230.
17
18
19 20. Mhanna, R.; Lefort, R.; Noirez, L.; Morineau, D., Microstructure and Concentration
20 Fluctuations in Alcohol-Toluene and Alcohol-Cyclohexane Binary Liquids: A Small Angle
21 Neutron Scattering Study. *Journal of Molecular Liquids* **2016**, *218*, 198-207.
22
23
24 21. Hamid, A. R. A.; Mhanna, R.; Lefort, R.; Ghoufi, A.; Alba-Simionesco, C.; Frick, B.;
25 Morineau, D., Microphase Separation of Binary Liquids Confined in Cylindrical Pores. *Journal*
26 *of Physical Chemistry C* **2016**, *120* (17), 9245-9252.
27
28
29 22. Mhanna, R.; Hamid, A.; Dutta, S.; Lefort, R.; Noirez, L.; Frick, B.; Morineau, D.,
30 More Room for Microphase Separation: An Extended Study on Binary Liquids Confined in
31 SBA-15 Cylindrical Pores. *Journal of Chemical Physics* **2017**, *146* (2).
32
33
34 23. Dutta, S.; Lefort, R.; Morineau, D.; Mhanna, R.; Merdrignac-Conanec, O.; Saint-
35 Jalmes, A.; Leclercq, T., Thermodynamics of Binary Gas Adsorption in Nanopores. *Physical*
36 *Chemistry Chemical Physics* **2016**, *18* (35), 24361-24369.
37
38
39 24. Essafri, I.; Morineau, D.; Ghoufi, A., Microphase Separation of a Miscible Binary Liquid
40 Mixture under Confinement at the Nanoscale. *Npj Computational Materials* **2019**, *5*.
41
42
43
44
45
46
47
48
49
50
51
52
53
54
55
56
57
58
59
60

- 1
2
3 25. Hamid, A. R. A.; Mhanna, R.; Catrou, P.; Bulteau, Y.; Lefort, R.; Morineau, D.,
4 Multiple Glass Transitions of Microphase Separated Binary Liquids Confined in MCM-41.
5
6 *Journal of Physical Chemistry C* **2016**, *120* (20), 11049-11053.
7
8
9
10 26. Zhao, D.; Huo, Q.; Feng, J.; Chmelka, B.; Stucky, G., Nonionic Triblock and Star
11 Diblock Copolymer and Oligomeric Surfactant Syntheses of Highly Ordered, Hydrothermally
12 Stable, Mesoporous Silica Structures. *Journal of the American Chemical Society* **1998**, *120* (24),
13 6024-6036.
14
15
16
17
18
19 27. Dosseh, G.; Brodie-Linder, N.; Frick, B.; Le Quellec, C.; Morineau, D.; Alba-
20 Simionescu, C., Dynamical Properties of Toluene and ortho-Terphenyl Confined in MCM-41
21 and SBA-15 Mesoporous Materials. *Annales De Chimie-Science Des Materiaux* **2005**, *30* (4),
22 365-373.
23
24
25
26
27
28 28. Xia, Y. D.; Dosseh, G.; Morineau, D.; Alba-Simionescu, C., Phase Diagram and Glass
29 Transition of Confined Benzene. *Journal of Physical Chemistry B* **2006**, *110* (39), 19735-19744.
30
31
32
33 29. Brodie-Linder, N.; Dosseh, G.; Alba-Simionescu, C.; Audonnet, F.; Imperor-Clerc, M.,
34 SBA-15 synthesis: Are there Lasting Effects of Temperature Change within the First 10 min of
35 TEOS Polymerization? *Materials Chemistry and Physics* **2008**, *108* (1), 73-81.
36
37
38
39
40 30. Wuttke, J.; Budwig, A.; Drochner, M.; Kammerling, H.; Kayser, F.; Kleines, H.;
41 Ossovyi, V.; Pardo, L.; Prager, M.; Richter, D.; Schneider, G.; Schneider, H.; Staringer, S.,
42 SPHERES, Julich's High-Flux Neutron Backscattering Spectrometer at FRM II. *Review of*
43 *Scientific Instruments* **2012**, *83* (7).
44
45
46
47
48
49 31. Michaela, Z.; Marina, K., SPHERES: Backscattering Spectrometer. *Journal of large-*
50 *scale research facilities* **2015**, *A30*, 1-4.
51
52
53
54
55
56
57
58
59
60

- 1
2
3 32. Brodka, A.; Zerda, T., Properties of Liquid Acetone in Silica Pores: Molecular Dynamics
4 Simulation. *Journal of Chemical Physics* **1996**, *104* (16), 6319-6326.
5
6
7
8 33. Cygan, R.; Liang, J.; Kalinichev, A., Molecular Models of Hydroxide, Oxyhydroxide,
9 and Clay Phases and the Development of a General Force Field. *Journal of Physical Chemistry B*
10 **2004**, *108* (4), 1255-1266.
11
12
13
14 34. Jorgensen, W.; Maxwell, D.; TiradoRives, J., Development and Testing of the OPLS
15 All-Atom Force Field on Conformational Energetics and Properties of Organic Liquids. *Journal*
16 *of the American Chemical Society* **1996**, *118* (45), 11225-11236.
17
18
19
20 35. Forester, T. R.; Smith, W. DLPOLY, CCP5 Program Library; Daresbury Lab.,
21 Warrington, 2004.
22
23
24
25
26 36. Melchionna, S.; Ciccotti, G.; Holian, B., Hoover NPT Dynamics for Systems Varying in
27 Shape and Size. *Molecular Physics* **1993**, *78* (3), 533-544.
28
29
30
31 37. Smith, W.; Forester, T., DL_POLY_2.0: A General-Purpose Parallel Molecular
32 Dynamics Simulation Package. *Journal of Molecular Graphics* **1996**, *14* (3), 136-141.
33
34
35 38. McGregor, P. A.; Allan, D. R.; Parsons, S.; Clark, S. J., Hexamer Formation in Tertiary
36 Butyl Alcohol (2-Methyl-2-Propanol, C₄H₁₀O). *Acta Crystallographica Section B-Structural*
37 *Science* **2006**, *62*, 599-605.
38
39
40
41
42 39. Le Quellec, C.; Dosseh, G.; Audonnet, F.; Brodie-Linder, N.; Alba-Simionesco, C.;
43 Haussler, W.; Frick, B., Influence of Surface Interactions on the Dynamics of the Glass Former
44 ortho-Terphenyl Confined in Nanoporous Silica. *European Physical Journal-Special Topics*
45 **2007**, *141*, 11-18.
46
47
48
49
50
51 40. Marc, B., *Quasi-elastic Neutron Scattering Principles and Application in Solid State*
52 *Chemistry, Biology and Materials Science*. Adam Hilger, Bristol ed.; 1998.
53
54
55
56
57
58
59
60

- 1
2
3 41. Guégan, R.; Morineau, D.; Lefort, R.; Moréac, A.; Béziel, W.; Guendouz, M.;
4
5 Zanutti, J. M.; Frick, B., Molecular Dynamics of a Short-Range Ordered Smectic Phase
6
7 Nanoconfined in Porous Silicon. *Journal of Chemical Physics* **2007**, *126* (6).
- 8
9
10 42. Ndao, M.; Lefort, R.; Cerclier, C.; Busselez, R.; Morineau, D.; Frick, B.; Ollivier, J.;
11
12 Kityk, A.; Huber, P., Molecular Dynamics of Pyrene Based Discotic Liquid Crystals Confined in
13
14 Nanopores Probed by Incoherent Quasielastic Neutron Scattering. *Rsc Advances* **2014**, *4* (103),
15
16 59358-59369.
- 17
18
19 43. Zorn, R., On the Evaluation of Neutron Scattering Elastic Scan Data. *Nuclear*
20
21 *Instruments & Methods in Physics Research Section a-Accelerators Spectrometers Detectors and*
22
23 *Associated Equipment* **2009**, *603* (3), 439-445.
- 24
25
26 44. Hamid, A. R. A.; Lefort, R.; Lechaux, Y.; Moreac, A.; Ghoufi, A.; Alba-Simionesco,
27
28 C.; Morineau, D., Solvation Effects on Self-Association and Segregation Processes in tert-
29
30 Butanol-Aprotic Solvent Binary Mixtures. *Journal of Physical Chemistry B* **2013**, *117* (35),
31
32 10221-10230.
- 33
34
35 45. Hennous, L.; Hamid, A.; Lefort, R.; Morineau, D.; Malfreyt, P.; Ghoufi, A., Crossover
36
37 in Structure and Dynamics of a Primary Alcohol Induced by Hydrogen-Bonds Dilution. *Journal*
38
39 *of Chemical Physics* **2014**, *141* (20).
- 40
41
42 46. Donth, E., The Size of Cooperatively Rearranging Regions at the Glass-Transition.
43
44 *Journal of Non-Crystalline Solids* **1982**, *53* (3), 325-330.
- 45
46
47 47. Ediger, M. D.; Angell, C. A.; Nagel, S. R., Supercooled Liquids and Glasses. *Journal of*
48
49 *Physical Chemistry* **1996**, *100* (31), 13200-13212.
- 50
51
52 48. Tracht, U.; Wilhelm, M.; Heuer, A.; Feng, H.; Schmidt-Rohr, K.; Spiess, H. W.,
53
54 Length Scale of Dynamic Heterogeneities at the Glass Transition Determined by
55
56
57
58
59
60

- 1
2
3 Multidimensional Nuclear Magnetic Resonance. *Physical Review Letters* **1998**, *81* (13), 2727-
4
5 2730.
6
7
8 49. Ediger, M., Spatially Heterogeneous Dynamics in Supercooled Liquids. *Annual Review*
9
10 *of Physical Chemistry* **2000**, *51*, 99-128.
11
12 50. Zorn, R.; Hartmann, L.; Frick, B.; Richter, D.; Kremer, F., Inelastic Neutron Scattering
13
14 Experiments on the Dynamics of a Glass-Forming Material in Mesoscopic Confinement. *Journal*
15 *of Non-Crystalline Solids* **2002**, *307*, 547-554.
16
17
18 51. Dosseh, G.; Le Quellec, C.; Brodie-linder, N.; Alba-simionesco, C.; Haeussler, W.;
19
20 Levitz, P., Fluid-Wall Interactions Effects on the Dynamical Properties of Confined
21
22 Orthoterphenyl. *Journal of Non-Crystalline Solids* **2006**, *352* (42-49), 4964-4968.
23
24
25 52. Scheidler, P.; Kob, W.; Binder, K., Cooperative Motion and Growing Length Scales in
26
27 Supercooled Confined Liquids. *Europhysics Letters* **2002**, *59* (5), 701-707.
28
29
30 53. Lefort, R.; Morineau, D.; Guegan, R.; Guendouz, M.; Zanotti, J. M.; Frick, B.,
31
32 Relation between Static Short-range Order and Dynamic Heterogeneities in a Nanoconfined
33
34 Liquid Crystal. *Physical Review E* **2008**, *78* (4).
35
36
37 54. Scheidler, P.; Kob, W.; Binder, K., The Relaxation Dynamics of a Confined Glassy
38
39 Simple Liquid. *European Physical Journal E* **2003**, *12* (1), 5-9.
40
41
42 55. Ji, Q.; Lefort, R.; Busselez, R.; Morineau, D., Structure and Dynamics of a Gay-Berne
43
44 Liquid Crystal Confined in Cylindrical Nanopores. *Journal of Chemical Physics* **2009**, *130* (23).
45
46
47 56. Busselez, R.; Lefort, R.; Ji, Q.; Affouard, F.; Morineau, D., Molecular Dynamics
48
49 Simulation of Nanoconfined Glycerol. *Physical Chemistry Chemical Physics* **2009**, *11* (47),
50
51 11127-11133.
52
53
54
55
56
57
58
59
60

- 1
2
3 57. Ghoufi, A.; Hureau, I.; Morineau, D.; Renou, R.; Szymczyk, A., Confinement of tert-
4 Butanol Nanoclusters in Hydrophilic and Hydrophobic Silica Nanopores. *Journal of Physical*
5 *Chemistry C* **2013**, *117* (29), 15203-15212.
6
7
8
9
10 58. Guégan, R.; Morineau, D.; Alba-Simionesco, C., Interfacial Structure of an H-Bonding
11 Liquid Confined into Silica Nanopore with Surface Silanols. *Chemical Physics* **2005**, *317* (2-3),
12 236-244.
13
14
15
16
17 59. Guo, X. Y.; Watermann, T.; Sebastiani, D., Local Microphase Separation of a Binary
18 Liquid under Nanoscale Confinement. *Journal of Physical Chemistry B* **2014**, *118* (34), 10207-
19 10213.
20
21
22
23
24 60. Lerbret, A.; Lelong, G.; Mason, P. E.; Saboungi, M. L.; Brady, J. W., Molecular
25 Dynamics and Neutron Scattering Study of Glucose Solutions Confined in MCM-41. *Journal of*
26 *Physical Chemistry B* **2011**, *115* (5), 910-918.
27
28
29
30
31
32
33
34
35
36
37
38
39
40
41
42
43
44
45
46
47
48
49
50
51
52
53
54
55
56
57
58
59
60

TOC GRAPHIC

